COMMUNICATIONS IN SCIENCE AND TECHNOLOGY
Homepage: cst.kipmi.or.id

Preparation, synthesis and characterizations of $La_{0.7}Sr_{0.3}Mn_{(1-y)}Ni_{(y)}O_3$ alloy

Jan Setiawan[a,b], Ferry Budhi Susetyo[c,*], Dwi Nanto[d], Silviana Simbolon[e], Hamdan Akbar Notonegoro[f], Taufiq Al Farizi[d], Yunasfi[a], Dinda Tihera[g], Ramlan[g]

[a]*Research Center for Advanced Materials-National Research and Innovation Agency, Tangerang Selatan 15314, Indonesia*
[b]*Department of Electrical Engineering, Universitas Pamulang, Tangerang Selatan 15417, Indonesia*
[c]*Department of Mechanical Engineering, Universitas Negeri Jakarta, Jakarta 13220, Indonesia*
[d]*Department of Physic Education, Universitas Islam Negeri Syarif Hidayatullah, Jakarta 15412, Indonesia*
[e]*Department of Mechanical Engineering, Universitas Pamulang, Tangerang Selatan 15417, Indonesia*
[f]*Department of Mechanical Engineering, Universitas Sultan Ageng Tirtayasa, Cilegon 42118, Indonesia*
[g]*Department of Physics, Universitas Sriwijaya, Sumatera Selatan 30662, Indonesia*

Article history:
Received: 26 December 2023 / Received in revised form: 6 June 2024 / Accepted: 9 June 2024

Abstract

Nickel (Ni) doped in the perovskite manganite could result in superior properties. The effect of the Ni on the morphology, crystallographic orientation, and magnetic properties of $La_{0.7}Sr_{0.3}Mn_{(1-y)}Ni_{(y)}O_3$ alloy (y = 0.1, 0.3, 0.5, and 0.7), therefore, was undertaken. $La_{0.7}Sr_{0.3}Mn_{(1-y)}Ni_{(y)}O_3$ alloy was firstly processed using a ball milling process, and again processed through heat treatment and crushing at the end of the synthesis process. Powder alloy was then investigated using a scanning electron microscope equipped with scanning electron microscope and energy dispersive spectroscopy (SEM-EDS), x-ray diffraction (XRD), and vibrating sample magnetometer (VSM). The particle size became smaller and agglomerated as the amount of Ni doping increased. The polycrystal structure phase formed would become more complex when the Ni doping was 0.5 and 0.7, where the dominant phase formed was La_2NiO_4 even though the $La_{0.7}Sr_{0.3}Mn_{(1-y)}Ni_{(y)}O_3$ phase was still formed. The magnetic characteristics showed that the Ni doping of 0.1 had a higher magnetization value around 4.2 emu/g at room temperature.

Keywords: Morphology; polycrystal structure phase; magnetic properties

1. Introduction

Perovskite manganite has become an interesting topic for advance material investigation for having complex and superior properties that show unique morphology, crystallographic orientation, and magnetic behavior [1–3]. Many applications, therefore, may apply it, such as magnetocaloric, sensor, memory, and biomedical [4–7]. Moreover, perovskite manganite could be synthesized through several commonly used methods including sol-gel [6], solid-state reaction [8], auto-combustion [9], and milling [10]. From several methods mentioned above, milling seems the best candidate for synthesis due to its ability to achieve lower particle size at room temperature operating conditions [11]. Moreover, Manh et al.'s combination synthesis process using milling followed by various heat treatments resulted in the promising properties of the perovskite manganite, such as lower crystallite size [12].

In addition to synthesis methods, the type of material doped into the perovskite manganite could also be promising superior properties of the alloy (such as Ni) [13]. For this, several researchers added the small amount of Ni to the alloy. Ginting *et al.* added Ni into the $La_{0.7}Sr_{0.3}Mn_{1-x}Ni_xO_3$ (x = 0.01, 0.02, and 0.03), resulting in a single phase in a rhombohedral perovskite structure [14]. Gupta *et al.* added Ni into the $La_{0.67}Sr_{0.33}Mn_{1-x}Ni_xO_3$ ($0.00 \leq x \leq 0.09$), shifting to more Ni content, and resulting in a decrease in lattice parameters [15]. Gomez *et al.* added Ni into the $La_{0.7}Ca_{0.3}Mn_{1-x}Ni_xO_3$ (x = 0, 0.02, 0.07, and 0.1), increasing the Ni in the alloy, and promoting a decrease in crystallite size [9]. In contrast, Cetin *et al.* doped Ni into $La_{0.7}Sr_{0.3}Mn_{1-x}Ni_xO_3$ ($0.00 \leq x \leq 0.06$)), increasing the Ni composition and leading to an increase in crystallite size [16]. Moreover, Thamilmaran *et al.* added Ni into the $La_{0.7}Sr_{0.3}Ni_xMn_{1-x}O_3$ (x = 0.01, 0.02, and 0.03), shifting to more Ni content, and resulting in an increase in the density of the alloy and a decrease in average particle size [8]. Oumezzi *et al.* added Ni into the $La_{0.6-x}Pr_{0.1}Ba_{0.3}Mn_{1-x}Ni_xO_3$ ($0 \leq x \leq 0.3$) and found that enhanced Ni content led to a decrease in lattice parameter [17]. Ran *et al.* doped Ni to $LaMn_{1-x}Ni_xO_3$ perovskites (x = 0.1,0.2, and 0.3) and found an increase in the average valence of Mn by increasing the Ni-

* Corresponding author.
Email: fbudhi@unj.ac.id
https://doi.org/10.21924/cst.9.1.2024.1361

doped amount [18]. A study by Handal *et al.* showed that the smallest crystallite size affected resulting higher magnetization (*Ms*) value [19]. Moreover, the decrease in particle size contributed to the decrease of the *Ms* value [20,21].

Based on the several researchers findings above, many aspects need further exploration, especially for $La_{0.7}Sr_{0.3}Mn_{(1-y)}Ni_{(y)}O_3$ alloy (y = 0.1, 0.3, 0.5, and 0.7). Several researchers doped Ni in the $La_{0.7}Sr_{0.3}Mn_{(1-x)}Ni_{(x)}O_3$ ($x \leq 0.3$) [8,14,16]. Therefore, in the present study, $La_{0.7}Sr_{0.3}Mn_{(1-y)}Ni_{(y)}O_3$ alloy (y = 0.1, 0.3, 0.5, and 0.7) prepared by milling and crystallized through heat treatment was undertaken. The powder alloy was then investigated using a scanning electron microscope equipped with scanning electron microscope and energy dispersive spectroscopy (SEM-EDS), x-ray diffraction (XRD), and vibrating sample magnetometer (VSM) to study the effect of the Ni on the morphology, crystallographic orientation, and magnetic properties.

2. Materials and Methods

La_2O_3, $SrCO_3$, MnO_2, and NiO powder (5µm) analytical grades obtained from Merck were used in the present research. $La_{0.7}Sr_{0.3}Mn_{(1-y)}Ni_{(y)}O_3$ alloy (y = 0.1, 0.3, 0.5, and 0.7) was first processed using a ball milling process. La_2O_3, $SrCO_3$, MnO_2, and MnO powder were mixed with acetone in the vial and milling for 300 min. Subsequently, the mixed powder was heated at 80°C for 720 minutes (air condition). The mixed dried powder was then compacted and sintered at 1200°C for 720 minutes (air condition). The sintered sample was crushed and used for SEM-EDS, XRD, and VSM investigations. Fig. 1 presents the complete sample preparation and synthesis.

XRD investigation was conducted using step size 0.02°. PANalytical AERIS equipment with Cu$K\alpha$ radiation (λ=1.5406 Å) was used for XRD investigation. Collected XRD data was refined using Highscore Plus software. Also, SEM JEOL JSM 6510 equipped with EDS was used for morphology and elemental investigation. Three images were taken in different locations using SEM at 5000x magnification. From these three images, analysis was conducted using ImageJ to determine the particle size. From this analysis, the distribution of particle size diagrams was constructed. VSM250 (up to 20kOe external magnetic field) was used to investigate magnetic properties.

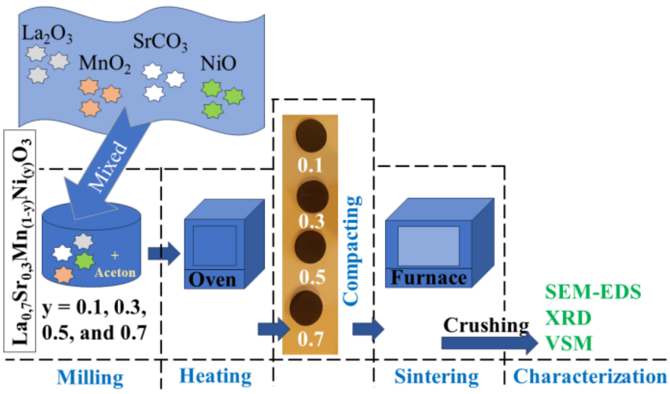

Fig. 1. Sample of preparation and synthesis

3. Results and Discussion

3.1. Morphology and Phase

Fig. 2 shows the morphology and phase spectrum based on SEM-EDS measurement. The morphology showed that the alloy powder was relatively larger. The tendency to agglomerate was also visible. According to the EDS spectrum, the elements La, Mn, and Sr dominate could be seen, and there were some Ni elements. The spectrum intensity was slightly lower than other for the Sr element (y = 0.1). This condition corroborated that the Sr doping occupancy was seen to be only 89%, while for other alloys, it was more than 90%. The Ni element could be observed in the range of 7 – 9 keV with the Ni*Ka* and Ni*Kb* spectra. The greater the Ni doping, the greater the spectrum intensity.

Table 1 shows the phase measurement results from EDS. It can be seen that Ni was perfectly doped in the $La_{0.7}Sr_{0.3}Mn_{(1-y)}Ni_{(y)}O_3$ alloy. Increasing the Ni-doped also increased the Ni phase in the alloy.

Table 1. Composition of element in Phase of $La_{0,7}Sr_{0,3}Mn_{(1-y)}Ni_{(y)}O_3$ alloy from EDS investigation

Element	y			
	0.1	0.3	0.5	0.7
La	50.66	31.09	30.51	28.26
Sr	13.97	25.89	26.81	32.74
Mn	21.83	24.71	21.44	10.66
Ni	8.92	10.87	15.39	21.49
O	4.61	7.45	5.84	6.85

Fig. 3 represents the average particle size, and the size dispersion was estimated using Gaussian fitting and distribution of FWHM [22]. More Ni-doped resulted in a decrease in particle size, which is in perfect agreement with other studies [8,23]. Different phenomenon in Pena-Garcia et al. showed that Ni-doped in the hexagonal structure caused the strain value of the lattice, which contributed to an increase in particle size [24].

From the distribution of these particles, differences in the size distribution of the particles formed can be seen Fig. 3(a) showing that the distribution was skewed to the right. The highest particle distribution was in the range of 300–400 nm with a few particles with a distribution in the range of 500–600 nm. Different from Fig. 3(b), the largest particles were in a range similar to Fig. 3(a) but tended to increase in particle size in the range of 200–300 nm, followed by a decrease in particle size in the range of 400–500 nm. In Fig. 3(c), it can also be seen that the highest distribution tended to shift to a lower range. The highest particle distribution was in the range of 200–300 nm. The tendency of particle distribution to decrease can be seen in Fig. 3(d) with the increasing number of particles in the range 200–300 nm and the small amount of particles in other ranges.

3.2. Crystallographic Orientation

Fig. 4 shows the spectrum based on XRD measurement.

According to Fig. 4, if each peak in the sample was fitted to the peak on the ICSD database card 98-005-5965 for $LaMnO_3$ with a hexagonal structure (R -3 c space group), there was a very strong additional complex phase at y = 0.5 and 0.7. In contrast, Ni-doped (y = 0.1 and 0.3) still showed a single phase in accordance with the database for $LaMnO_3$ with a hexagonal crystal structure (R -3 c space group). However, the peak intensity of the two alloys was found lower and wider. Thus, the doping of the Ni changed the phase formation in lanthanum manganite.

Four phases could approximate the suitable phases for the diffraction patterns of Ni-doped 0.5 and 0.7. The first phase was $La_{0.7}Sr_{0.3}Mn_{(1-y)}Ni_{(y)}O_3$ (y = 0.5 and 0.7). The second phase was NiO, which had a cubic crystal structure with a space group F m -3 m. The third phase was La_2NiO_4 with a tetragonal crystal structure and had space group I 4/m m m. The fourth phase was $Sr_4Mn_2NiO_9$, which had a hexagonal crystal structure with space group P 3 2 1.

Furthermore, for the crystallographic analysis of the diffraction pattern, Rietveld analysis was carried out using the Highscore Plus software with suitable phase information input data. Table 2 presents the Rietveld analysis summary results for all diffraction patterns. The information provided can include lattice parameter data, Ni doping occupancy, and statistical parameters from the Rietveld analysis carried out.

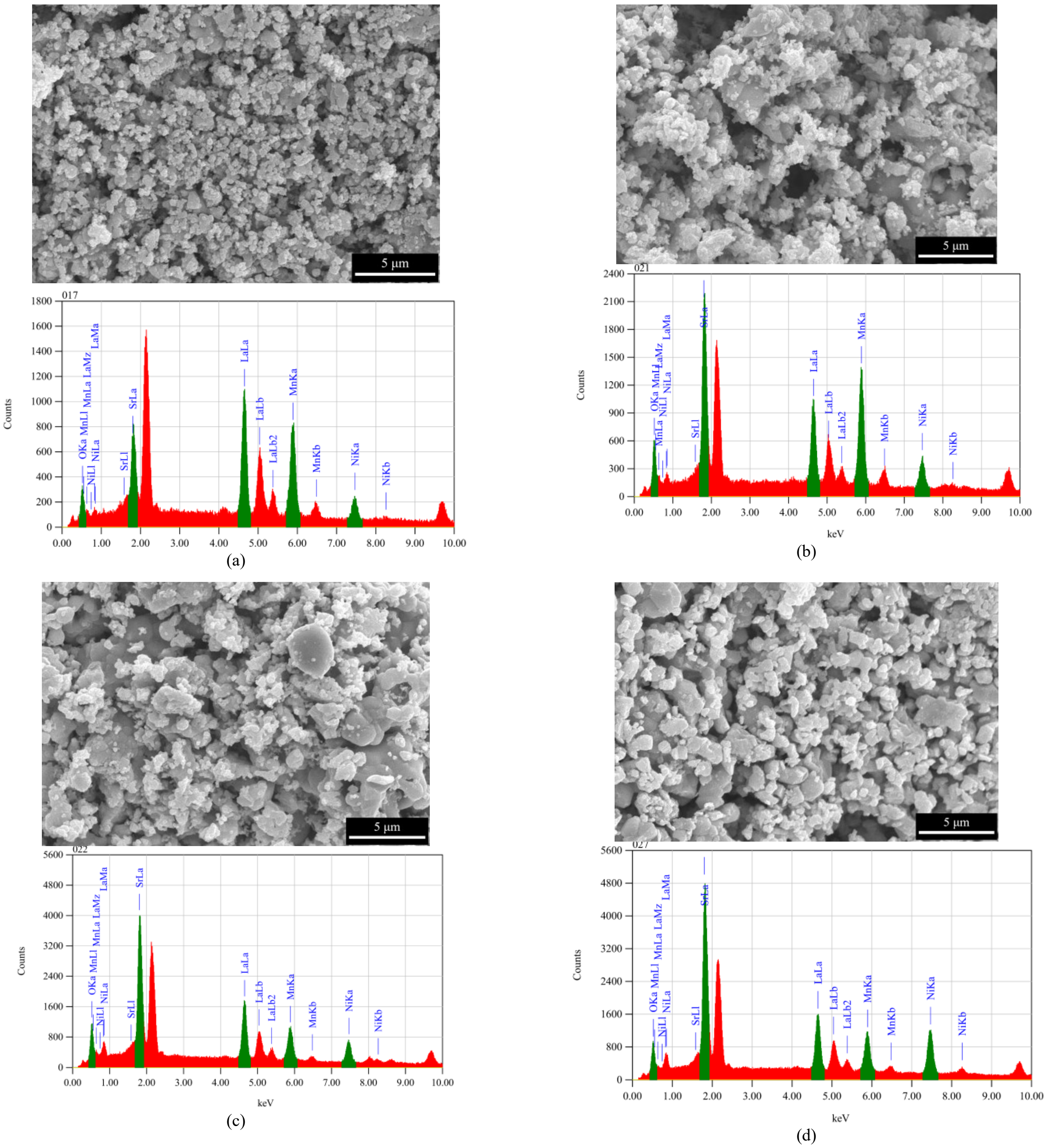

Fig. 2. Morphology and Phase of $La_{0,7}Sr_{0,3}Mn_{(1-y)}Ni_{(y)}O_3$ alloy (a) y=0.1, (b) y=0.3, (c) y=0.5, and (d) y=0.7

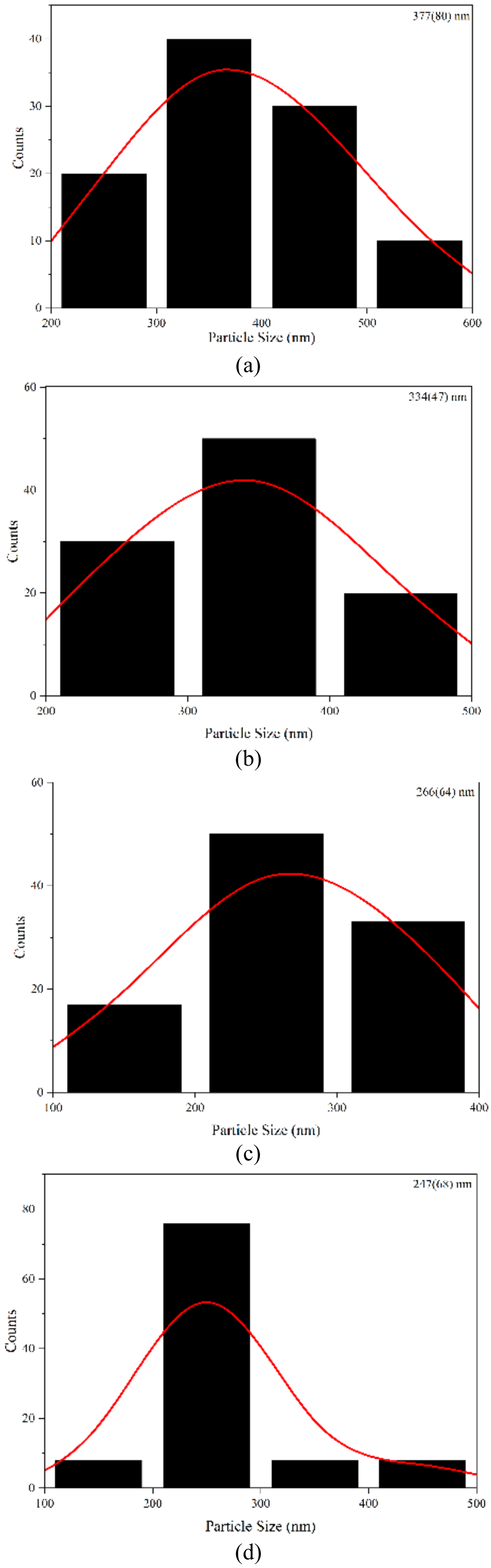

Fig. 3. Particle size of $La_{0,7}Sr_{0,3}Mn_{(1-y)}Ni_{(y)}O_3$ alloy (a) y=0.1, (b) y=0.3, (c) y=0.5, and (d) y=0.7

Table 2. Crystallographic orientation of $La_{0,7}Sr_{0,3}Mn_{(1-y)}Ni_{(y)}O_3$ alloy from XRD refinement

	Y			
	0.1	0.3	0.5	0.7
Crystal system	Hexagonal			
Space group	R -3 c			
Lattice parameter				
a = *b* (Å)	5.4540	5.4507	5.4286	5.4077
c (Å)	13.3351	13.2747	13.26357	13.2465
Volume (Å^3)	343.521	341.550	338.512	335.470
Crystallite size (Å)	224	257	288	541
Density (g/cm^3)	6.63	6.65	6.72	6.81
Strain	0.015	0.045	0.064	0.109
Occupancy				
La	0.7321	0.7057	0.7060	0.7103
Sr	0.2679	0.2943	0.2940	0.2897
Mn	0.9303	0.7055	0.5114	0.3612
Ni	0.0697	0.2945	0.4886	0.6388
Weight (%)	100.0	100.0	22.1	7.2
			NiO	
Crystal system			Cubic	
Space group			F m -3 m	
Lattice parameter				
a = *b* = *c* (Å)			4.1069	4.1729
Volume (Å^3)			69.2713	72.6603
Weight (%)			14.2	12.2
			La_2NiO_4	
Crystal system			Tetragonal	
Space group			I 4/m m m	
Lattice parameter				
a = *b* (Å)			3.7620	3.8245
c (Å)			12.2446	12.5087
Volume (Å^3)			173.2926	182.9579
Weight (%)			43.4	58.1
			$Sr_4Mn_2NiO_9$	
Crystal system			Hexagonal	
Space group			P 3 2 1	
Lattice parameter				
a = *b* (Å)			9.5477	9.5738
c (Å)			7.5725	7.7533
Volume (Å3)			597.8181	615.4437
Weight (%)			20.3	22.5
Statistical parameter				
Goodness of fit	5.0221	3.5679	38.7922	30.9422
Rp	2.8124	2.5335	7.1231	2.0559
Rwp	4.0843	3.6615	12.2883	11.4362

As shown in Table 2, a, b, and c lattice parameters and volume decreased with an increase in the doped Ni, which is in agreement with another report [15,25]. This showed that the oxidation number of Ni in this alloys was Ni^{3+} [25]. This behavior was attributed to the formation of a larger proportion of Mn^{4+} with respect to Mn^{3+} [17]. Moreover, it can be seen that an increase in the Ni-doped led to an increase in the density of the alloy. Thamilmaran *et al*. stated that the tight packing of the material and the doping level of the Ni influenced the density occurred [8].

Increased Ni-doped concentration led to increased crystallite size (see Table 2), which is in perfect agreement with others researchers [16,26]. According to Pena-Garcia *et al*., there is a correlation between crystallite size and strain in the lattice [27]. It can be seen that strain increases due to increases in Ni-doped (see Table 2). Therefore, it can be concluded that an increase in strain leads to increased crystallite size.

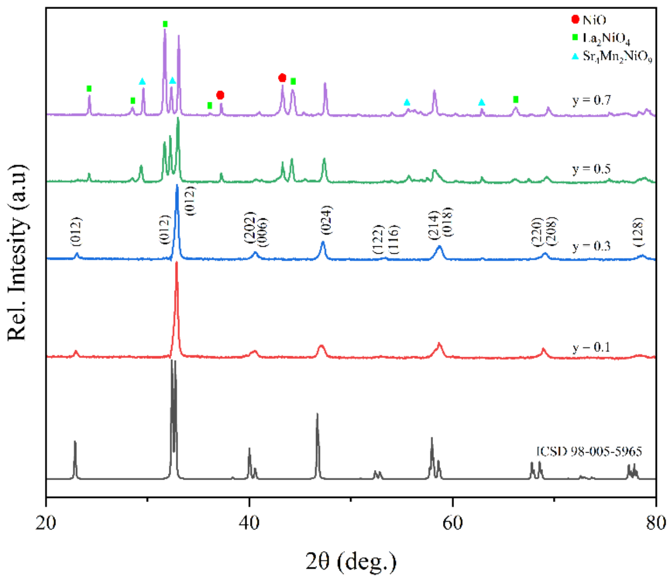

Fig. 4. XRD Spectrum of $La_{0,7}Sr_{0,3}Mn_{(1\text{-}y)}Ni_{(y)}O_3$ alloy

3.3. Magnetic Properties

Magnetic properties curve based on VSM measurement can be seen in Fig. 5 and Fig. 6. The magnetic characteristic test results as shown in Fig. 5 and Fig.6 showed that the Ms value for Ni doping was 0.1 higher than other alloys, probably due to the smallest crystallite size and larger particle size. Handal et al. found that the smallest crystallite size affected higher Ms [19]. Compared to the XRD refinement, the smallest crystallite size was seen in a Ni-doped of 0.1. The decrease in particle size also contributed to the decrease of the Ms [20,21].

As shown in Fig. 5, the alloy with a Ni-doped of 0.1 had an initial magnetization of 0.374 emu/g. According to Fig. 6, the magnitude of the *Ms* in the alloy with Sr doping of 0.1 was 4.20 emu/g. Increasing the doped of Ni led to a decrease in the Ms (see Table 3), which perfectly agreed with the study of Gupta *et al.* and Creel *et al.* [15,25]. Another study investigated by Gupta *et al.* also found a similar behavior [28]. According to Gupta *et al.*, a decrease in *Ms* was due to antiferromagnetic alignment [15].

The comparison parameter *Mr*/*Ms* was 0.090 with a loop area as shown in the inset of Fig. 6, which was enlarged in the external magnetic field range of 0.2 T (2000 Oe) of 251.7 kOe.emu/g. The mechanism for changing the magnetic value of the $La_{0.7}Sr_{0.3}Mn_{(1\text{-}y)}Ni_{(y)}O_3$ alloy was greatly determined by the amount of Sr and Ni doping, which would provide the optimum magnetization value. Pena-Garcia *et al*. found that Sr would result in the lowest magnetic moment and a Ni contribution for paramagnetic [24]. Moreover, there are compositions with certain values that can provide maximum magnetic characteristics, but other compositions that may be higher will reduce the magnetic characteristics [29].

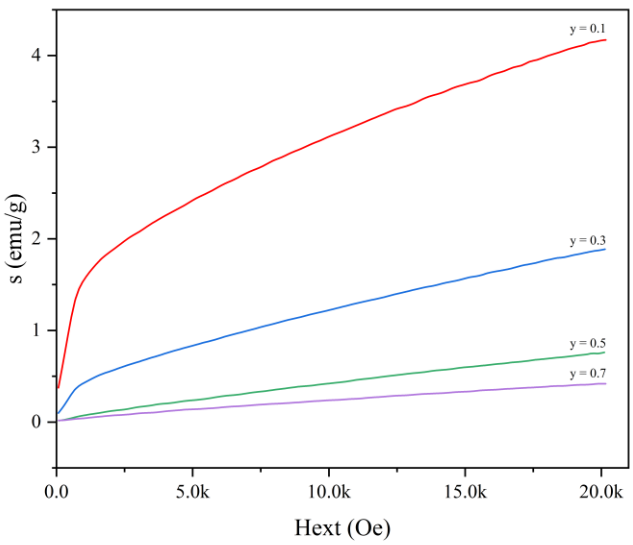

Fig. 5. Magnetization of $La_{0.7}Sr_{0.3}Mn_{(1\text{-}y)}Ni_{(y)}O_3$ alloy at room temperature.

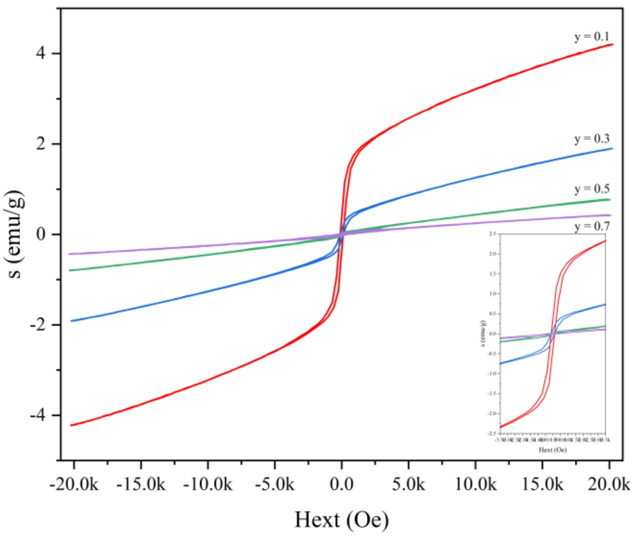

Fig. 6. Hysteresis curve of $La_{0.7}Sr_{0.3}Mn_{(1\text{-}y)}Ni_{(y)}O_3$ alloy at room temperature.

Moreover, Ni doping caused the remanen (*Mr*) to decrease (see Table 3). Changes in the magnetic properties of the system would determine the intrinsic and extrinsic factors. Intrinsic factors were viewed from changes in magnetic interactions, which can be explained as double ferromagnetic exchange interactions (Mn^{3+}-O-Mn^{4+}) or changes in internal structure. In contrast, extrinsic factors appeared in the form of particle size changes or the presence of an impurity phase [30]. For $y < 0.31$, the moments of Ni^{3+} aligned antiferromagnetically with the ferromagnetic coupled Mn^{3+} and Mn^{4+}. Meanwhile, $y \geq 0.31$ antiferromagnetic coupling between Ni^{3+} and Mn^{4+} moments became more dominant, resulting in an antiferromagnetic state [25]. In addition, the formation of the NiO, $Sr_4Mn_2NiO_9$ and La_2NiO_4 phases indicated the presence of antiferromagnetic chains [25,31–33].

Partial doping of Mn-sites with Ni^{2+} ions weakened the ferromagnetic properties by reducing the Mn^{3+}-O-Mn^{4+}

double exchange interaction. The double exchange between Mn^{3+} and Mn^{4+} mediated the ferromagnetism and conductance of metals [14,15,34]. Additional Ni^{2+} was introduced into the sample, occupying Mn sites randomly in the lattice, which no longer efficiently participated in the double exchange process and increased the ratio of Mn^{4+} ions in the lattice. Thus, antiferromagnetic interactions were formed, Mn^{3+}-O-Ni^{2+}, Mn^{4+}-O-$Mn^{4+,}$ and Ni^{2+}-O-Ni^{2+}, which were super exchange interactions providing antiferromagnetic contributions [9,14,15,34,35]. It should be noted that the double exchange between Mn^{3+} and Mn^{4+} mediated the ferromagnetism and conductance of metals. The larger influence to the magnetic properties, in this case were from the charge ordering and magnetic coupling compared to the appearance of the NiO phase [25].

Table 3. Magnetic properties of $La_{0,7}Sr_{0,3}Mn_{(1-y)}Ni_{(y)}O_3$ alloy from VSM investigation

y	*Ms* (emu/g)	*Mr* (emu/g)	*Hc* (Oe)
0.1	4.2	0.38	8.8
0.3	1.9	0.1	118.9
0.5	0.78	0.02	198.2
0.7	0.43	0.02	29.9

The value of Ms for Ni = 0.1 was much smaller than the value reported by Gupta *et al*., where for Ni = 0.15 and 0.25, the value of Ms was at 9.5 and 5.5 emu/g, respectively [28]. Also, the study reported by Creel et al. showed the value of Ms was 20.42 emu/g for Ni = 0.31 reaching at 9T [25]. For Ni = 0.5 and 0.7, the value of Ms was meagre because the phase was not only $La_{0.7}Sr_{0.3}Mn_{(1-y)}Ni_{(y)}O_3$; other phases existed with antiferromagnetic characteristics [25,33].

4. Conclusion

The $La_{0.7}Sr_{0.3}Mn_{(1-y)}Ni_{(y)}O_3$ alloy can be synthesized well using milling and crystallized through heat treatment. The alloy particle size became smaller and agglomerated as the amount of Ni doping increased due to strains being formed. In terms of morphology and elemental content, the alloying elements can be detected well and reinforce each other with the results of XRD pattern analysis. Ni-doped of 0.1 and 0.3 produced a single phase, as expected. The phase formed became more complex when the Ni-doped was 0.5 and 0.7, where the dominant phase formed was La_2NiO_4 even though the $La_{0.7}Sr_{0.3}Mn_{(1-y)}Ni_{(y)}O_3$ phase was still formed. An increase in Ni-doped led to a decrease in lattice parameters and volume, inversely increasing crystallite size, density, and strain. The magnetization value for Ni doping was 0.1 higher than other alloys due to the lowest crystallite size and larger particle size.

Acknowledgements

This research was financially supported by the Ministry of Education, Culture, Research and Technology of Indonesia in 2023 with contract number 180/E5/PG.02.00.PL/2023; 021/SP2H/RT-MONO/LL4/2023; 107/D5/SK/LPPM/UNPAM/VII/2023. DN and TAF thanks to research grant of UIN Syarif Hidayatullah No. Un. 01/KPA/59/2024.

References

1. P. Sfirloaga, M. Poienar, I. Malaescu, A. Lungu and P. Vlazan, *Perovskite type lanthanum manganite: Morpho-structural analysis and electrical investigations*, J. Rare Earths 36 (2018) 499–504.
2. N. S. Fedorova, Y. W. Windsor, C. Findler, M. Ramakrishnan, A. Bortis, L. Rettig et al., *Relationship between crystal structure and multiferroic orders in orthorhombic perovskite manganites*, Phys. Rev. Mater. 2 (2018) 1–16.
3. R. Rao, Y. Y. Han, X. C. Kan, X. Zhang, M. Wang, N. X. Qian et al., *Magnetic property under the pressure and electrical transport behavior under the magnetic field for the perovskite manganite La0.7Ca0.3MnO3*, J. Alloys Compd. 837 (2020) .
4. R. Hamdi, S. Boulfrad, S. S. Hayek, A. Samara, S. A. Mansour and Y. Haik, *Comparative analysis of the structural, magnetic, and magnetocaloric properties of Gd0.5Dy0.5Mn0.5X0.5O3 (X = Ni, Fe, and Co) nanoparticles*, Inorg. Chem. Commun. 158 (2023) 111589.
5. G. Kandasamy, *Recent advancements in manganite perovskites and spinel ferrite-based magnetic nanoparticles for biomedical theranostic applications*, Nanotechnology 30 (2019) 502001.
6. S. Yang, Q. Chen, Y. Yang, Y. Gao, R. Xu, H. Zhang et al., *Silver addition in polycrystalline La0.7Ca0.3MnO3: Large magnetoresistance and anisotropic magnetoresistance for manganite sensors*, J. Alloys Compd. 882 (2021) .
7. C. H. Lai and T. Y. Tseng, *Preparation and properties of perovskite thin films for resistive nonvolatile memory applications*, Ferroelectrics 357 (2007) 17–27.
8. P. Thamilmaran, M. Arunachalam, S. Sankarrajan and K. Sakthipandi, *Impact of Ni doping on La0.7Sr0.3NixMn1-xO3 perovskite manganite materials*, J. Magn. Magn. Mater. 396 (2015) 181–189.
9. A. Gómez, E. Chavarriaga, I. Supelano, C. A. Parra and O. Morán, *Tuning the magnetocaloric properties of La0.7Ca0.3MnO3 manganites through Ni-doping*, Phys. Lett. Sect. A Gen. At. Solid State Phys. 382 (2018) 911–919.
10. A. D. Souza, S. Rayaprol, M. S. Murari and M. Daivajna, *Effect of milling on structure and magnetism of nanocrystalline La0.7-xBixSr0.3MnO3 (x = 0.35, 0.40) manganites*, Phys. B Phys. Condens. Matter 606 (2021) 412792.
11. G. C. Figueroa, Ó. A. Olmos, A. G. Garcés, J. A. O. Vélez, J. J. Beltrán, E. B. Miranda et al., *Influence of Ball Milling Process on Structural and Magnetic Properties of OF La0.7Sr0.3MnO3 Manganite*, Rev. EIA 11 (2014) 31–38.
12. D. H. Manh, P. T. Phong, P. H. Nam, D. K. Tung, N. X. Phuc and I. J. Lee, *Structural and magnetic study of La0.7Sr0.3MnO 3 nanoparticles and AC magnetic heating characteristics for hyperthermia applications*, Phys. B Condens. Matter 444 (2014) 94–102.
13. N. Hamdaoui, D. Tlili, Y. Azizian-Kalandaragh, B. Zaidi, S. Zemni, A. A. Akl et al., *Effect of Ni-doping on the structural, magnetic, and electronic properties of La0.2Sr0.8MnO3 perovskite*, J. Mater. Sci. Mater. Electron. 32 (2021) 26984–26997.
14. D. Ginting, D. Nanto, Y. D. Zhang, S. C. Yu and T. L. Phan, *Influences of Ni-doping on critical behaviors of La0.7Sr 0.3Mn1-xNixO3*, Phys. B Condens. Matter 412 (2013) 17–21.
15. M. Gupta, R. K. Kotnala, W. Khan, A. Azam and A. H. Naqvi,

Magnetic, transport and magnetoresistance behavior of Ni doped La 0.67Sr0.33Mn1-xNixO3 (0.00≤x≤0.09) system, J. Solid State Chem. 204 (2013) 205–212.

16. S. Kılıç Çetin, G. Akça, M. S. Aslan and A. Ekicibil, *Role of nickel doping on magnetocaloric properties of La0.7Sr0.3Mn1−xNixO3 manganites*, J. Mater. Sci. Mater. Electron. 32 (2021) 10458–10472.
17. E. Oumezzine, S. Hcini, E. K. Hlil, E. Dhahri and M. Oumezzine, *Effect of Ni-doping on structural, magnetic and magnetocaloric properties of La0.6Pr0.1Ba0.3Mn1-xNixO3 nanocrystalline manganites synthesized by Pechini sol-gel method*, J. Alloys Compd. 615 (2014) 553–560.
18. R. Ran, X. Wu, D. Weng and J. Fan, *Oxygen storage capacity and structural properties of Ni-doped LaMnO 3 perovskites*, J. Alloys Compd. 577 (2013) 288–294.
19. H. T. Handal, H. A. Mousa, S. Mabrouk Yakout, W. Sharmoukh and V. Thangadurai, *Effect of Mn and Ni-doping on structure, photoluminescence and magnetic properties of perovskite-type BaSn0.99Gd0.01O3*, J. Magn. Magn. Mater. 498 (2020) 165946.
20. M. Jafari Eskandari and I. Hasanzadeh, *Size-controlled synthesis of Fe3O4 magnetic nanoparticles via an alternating magnetic field and ultrasonic-assisted chemical co-precipitation*, Mater. Sci. Eng. B 266 (2021) 115050.
21. F. Riyanti, H. Hasanudin, A. Rachmat, W. Purwaningrum and P. L. Hariani, *Photocatalytic degradation of methylene blue and Congo red dyes from aqueous solutions by bentonite-Fe3O4 magnetic*, Commun. Sci. Technol. 8 (2023) 1–9.
22. S. Schroeder, S. Braun, U. Mueller, R. Sonntag, S. Jaeger and J. P. Kretzer, *Particle analysis of shape factors according to American Society for Testing and Materials*, J. Biomed. Mater. Res. Part B Appl. Biomater. 108 (2020) 225–233.
23. S. Y. Lee, J. Yun and W. P. Tai, *Synthesis of Ni-doped LaSrMnO3 nanopowders by hydrothermal method for SOFC interconnect applications*, Adv. Powder Technol. 29 (2018) 2423–2428.
24. R. Peña-Garcia, Y. Guerra, S. Castro-Lopes, Y. M. Camejo, J. M. Soares, A. Franco et al., *Morphological, magnetic and EPR studies of ZnO nanostructures doped and co-doped with Ni and Sr*, Ceram. Int. 47 (2021) 28714–28722.
25. T. F. Creel, J. Yang, M. Kahveci, S. K. Malik, S. Quezado, O. A. Pringle et al., *Structural and magnetic properties of La0.7Sr0.3Mn1−xNixO3 (x ≤ 0.4)*, J. Appl. Phys. 114 (2013) 013911.
26. I. W. Risdianto, A. Ahmad and R. A. Ermawar, *Synthesis of cellulose acetate (CA) from algae Gracilaria sp. composited with nickel oxide (NiO) as a supercapacitor base material*, Commun. Sci. Technol. 8 (2023) 87–92.
27. R. Peña-Garcia, Y. Guerra, R. Milani, D. M. Oliveira, F. R. de Souza and E. Padrón-Hernández, *Influence of Ni and Sr on the structural, morphological and optical properties of ZnO synthesized by sol gel*, Opt. Mater. (Amst). 98 (2019) .
28. M. Gupta, W. Khan, P. Yadav, R. K. Kotnala, A. Azam and A. H. Naqvi, *Synthesis and evolution of magnetic properties of Ni doped La 2/3Sr 1/3Mn 1-xNi xO 3 nanoparticles*, J. Appl. Phys. 111 (2012) .
29. M. Eshraghi, H. Salamati and P. Kameli, *The effect of NiO doping on the structure, magnetic and magnetotransport properties of La0.8Sr0.2MnO3 composite*, J. Alloys Compd. 437 (2007) 22–26.
30. M. Oumezzine, O. Peña, T. Guizouarn, R. Lebullenger and M. Oumezzine, *Impact of the sintering temperature on the structural, magnetic and electrical transport properties of doped La 0,67Ba 0,33Mn 0,9Cr 0,1O 3 manganite*, J. Magn. Magn. Mater. 324 (2012) 2821–2828.
31. A. El Abed, E. Gaudin, S. Lemaux and J. Darriet, *Crystal structure and magnetic properties of Sr4Mn2NiO9*, Solid State Sci. 3 (2001) 887–897.
32. P. Stremoukhov, D. Carl S, A. Safin, S. Nikitov and A. Kirilyuk, *Phononic manipulation of antiferromagnetic domains in NiO*, New J. Phys. 24 (2022) 023009.
33. X. Batlle, X. Obradors, M. J. Sayagues, M. Vallet and J. Gonzalez-Calbet, *Weak ferromagnetism and magnetic interactions in La 2 NiO 4*, J. Phys. Condens. Matter 4 (1992) 487–496.
34. J. W. Feng, C. Ye and L. P. Hwang, *Magnetic and magnetotransport properties in the Ni-doped system*, Phys. Rev. B - Condens. Matter Mater. Phys. 61 (2000) 12271–12276.
35. A. E. M. A. Mohamed, B. Hernando and A. M. Ahmed, *Magnetic, magnetocaloric and thermoelectric properties of nickel doped manganites*, J. Alloys Compd. 692 (2017) 381–387.